Journal of Hydrology: Regional Studies 67 (2026) 103808

Contents lists available at ScienceDirect

Journal of Hydrology: Regional Studies

journal homepage: www.elsevier.com/locate/ejrh

Andean wetlands: Seasonal variability and their interactions with the cryosphere

Joshua Castro [a,*], Catriona L. Fyffe [b], Thomas E. Shaw [b], Evan S. Miles [a,c,d], Emily Potter [e], Martin Hoelzle [a], Vinisha Varghese [f], Francesca Pellicciotti [b]

[a] Department of Geosciences, University of Fribourg, Fribourg, Switzerland
[b] Institute of Science and Technology Austria, Austria
[c] Swiss Federal Institute for Forest, Snow and Landscape Research WSL, Birmensdorf, Switzerland
[d] Glaciology and Geomorphodynamics Group, Department of Geography, University of Zürich, Zürich, Switzerland
[e] School of Geography and Planning, University of Sheffield, Sheffield, UK
[f] Integrated Planning and Industrial Building, Institute of Building and Industrial Construction, Faculty of Civil and Environmental Engineering, TU Wien, Vienna, Austria

A R T I C L E I N F O

Keywords:
Andean wetlands
Wetlands seasonality
Seasonal snow cover

A B S T R A C T

Study region: The Vilcanota Urubamba Basin in southern Peru includes fragile wetland ecosystems that play a key role in mountain hydrology and support grazing for Andean communities.
Study focus: Mapping of wetlands variability is missing, limiting our understanding of their characteristics, seasonality and link with the cryosphere. We characterise wetland distribution, seasonality and persistence and evaluate their spatial association with glaciers and seasonal snow. Using Landsat 7 and 8 imagery, we build three-month seasonal land cover maps from 2013 to 2022 using a Random Forest classification and an Albedo Retrieval approach.
New hydrological insights for the region: Wetland area decreases by 38% from the end of the wet season (October to December) to the end of the dry season (July to September). Pixel transitions indicate that wetlands primarily transform to and from agricultural and pasture lands. Highly persistent wetlands are located above 4600 m a.s.l. and closer to glaciers than less persistent wetlands. We identified three wetland seasonal drying patterns. Basins with delayed and slow dry-out wetlands were more common at higher elevations but were not always in glacierised catchments, suggesting meltwater may maintain wetlands in the early dry season. We provide the first large-scale picture of wetland seasonality, and the basis for modelling the processes that sustain wetlands in tropical high mountains.

1. Introduction

The landscape of the Peruvian Andes is characterised by small, tropical glaciers that overlook expansive areas of lowland agricultural plains and pastures, inter-connected by zones of high elevation pasture and wetland (MINAM, 2018). This high Andean landscape is undergoing significant changes in the face of ongoing climatic change and variability (Cavieres et al., 2026; Poveda et al., 2020), which can affect the hydrological functioning of these mountain water towers (Buytaert et al., 2011). For example, snow and glaciers, which play a crucial role in storing and releasing water, have been undergoing rapid retreat over the last half century (e.g.

* Corresponding author.
E-mail address: joshua.castrocamacho@unifr.ch (J. Castro).

https://doi.org/10.1016/j.ejrh.2026.103808
Received 5 March 2026; Received in revised form 24 July 2026; Accepted 27 July 2026
Available online 30 July 2026

Seehaus et al., 2019). Peru contains ~73% of all tropical glacier areas (Turpo Cayo et al., 2022), which declined by 56% in area (1348 km^2) between 1962 and 2020 (INAIGEM 2023b), with a mass loss of −0.49 m w.e. yr^{-1} in the Cordillera Vilcanota over the last two decades (Taylor et al., 2022). Changes in runoff of water from glaciers and seasonal snow is therefore expected to affect the availability of water to downstream communities in lowland regions of Tropical Andes, especially during the dry seasons (Fyffe et al., 2025). However, an additional storage of water is afforded by the numerous high-elevation wetlands found in these hydro-climates, that experience seasonal changes in area, but support biodiversity and buffer dry-season water availability (Maldonado Fonkén, 2014; Ross et al., 2023). Some high-Andean wetlands function independently of direct cryospheric input (Wunderlich et al., 2023), while others rely on it (Gribbin et al., 2024). Crucially, however, the extent of their temporal and spatial dependency on glacier melt remains unclear (Polk et al., 2017; Cooper et al., 2019).

Analysis of land cover changes from remote sensing can provide assessment of seasonal variability in ecosystems, snow and glaciers. However, most studies to date have focused on the spatial extent of glaciers and their elevation changes over time (e.g., Fischer et al., 2015; Seehaus et al., 2019; Taylor et al., 2022), with less attention to the variability of ecosystems such as wetlands (e.g. Pizarro et al., 2022), particularly at finer temporal scales. Remote sensing studies that have attempted to explore wetland spatial variability remain constrained by limited temporal observation (e.g. Zakharova et al., 2014; Ross et al., 2023), relying on non-consecutive years or single seasonal snapshots. For instance, in Peru, national mapping efforts, such as the Ecosystem Map (MINAM, 2018), glacier inventories for 2016 and 2020 (INAIGEM, 2018, 2023b), and the National Inventory of Bofedales (INAIGEM 2023a), provide a useful initial representation of land cover distribution, but do not capture seasonal variability of wetlands or their spatial patterns. These temporal limitations hinder the understanding of how wetlands vary between seasons of a given year, and whether there is a connectivity between wetland area changes and the cryosphere or changes of land cover.

For this study, we focus on the Vilcanota-Urubamba basin (VUB) in southern Peru, which spans high-elevation, glacierised headwaters to lower-elevation forests and agriculture. In this basin, agriculture and hydropower depend on seasonal water availability, sustained by upstream meltwater, particularly during the dry season (Drenkhan et al., 2015), while seasonal meltwater availability in higher areas is regulated by precipitation through its effect on albedo and energy inputs (Fyffe et al., 2021). Wetlands in the VUB also provide essential ecosystem services supporting grazing, agricultural activities and the livelihoods in high-Andean communities (Postigo, 2014; Mazzarino, 2014). Given its sizable (> 5000 m) elevation range, pronounced seasonal precipitation variability, and critical role in sustaining water and ecosystems, the VUB offers an ideal setting for investigating seasonal

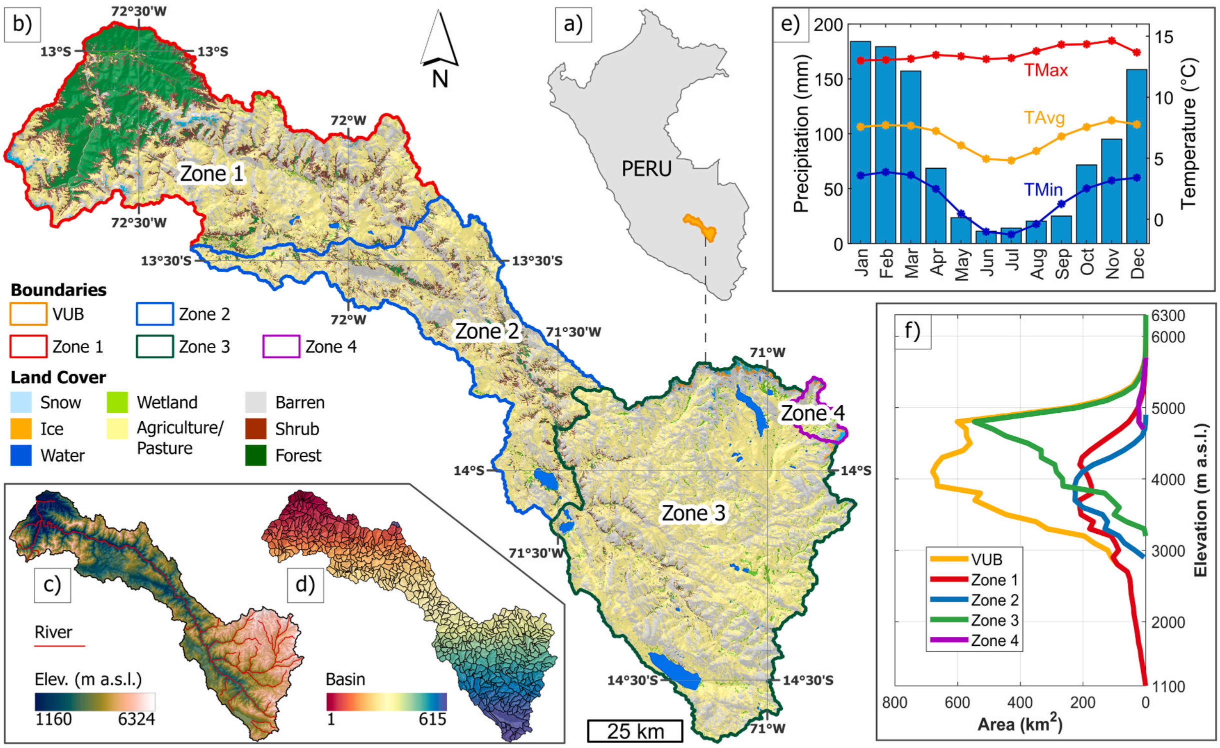

Fig. 1. Vilcanota-Urubamba Basin (VUB) study area. (a) Location of VUB within Peru. (b) Basin boundaries and zones, including land cover classes. (c) Elevation map including the Vilcanota-Urubamba River network from Instituto Geográfico Nacional (IGN, 2025), and (d) the 615 sub-basins computed inside VUB. (e) Monthly climograph of VUB during 2013–2022. (f) Histogram with the area distribution of VUB and its three zones. Zone 4 is shown for reference but not included in the basin-wide analysis. Land cover data correspond to our classification for July to September 2020. Climate information is derived from the gridded Weather Research and Forecasting (WRF) model (Potter et al., 2023). Elevation data are obtained from the 30 m SRTM V3 Digital Elevation Model (DEM) (Farr et al., 2007).

characteristics and variability of wetlands in the tropical mountains.

Our overall aim is to characterise the seasonal variability and persistence of wetlands within the VUB and the extent to which they are linked to the cryosphere. Specifically, we address: a) How do Andean wetlands vary spatially and seasonally across the VUB? and b) To what extent is wetland seasonality associated with glaciers and seasonal snow? To address these questions, we apply a Random Forest land cover classification at a three-month temporal resolution to Landsat imagery from 2013 to 2022. Our specific objectives are to 1) provide an assessment of the full extension of Andean land covers, as a baseline to establish a novel, time-varying and highly resolved inventory of wetlands every three months; and 2) analyse the spatial and seasonal variability of the land classes identified to provide the context for the changes in wetlands and their intricate relationships with the cryosphere.

2. Study site

The Vilcanota-Urubamba Basin (VUB) is located in the Cusco region of Peru (Fig. 1a), between 12.9°S to 14.6°S latitude and 70.8°W to 72.8°W longitude, within the Southern Wet Outer Tropics (Bonshoms et al., 2020). The basin is defined by the Vilcanota-Urubamba River, which originates in the southeastern region and flows toward the lower elevations in the northwest. Given its large area (> 11, 000 km^2) and wide elevation range, we divided the basin into three zones (Table 1) based on established boundaries of the glacierised mountain ranges (INAIGEM, 2018). Additionally, a fourth zone is introduced as a glacierised headwater case study in the Cordillera Vilcanota to support analysis on wetland and cryosphere connectivity at high elevations.

The VUB current land cover classification (MINAM, 2018) includes glaciers (1%) and sparsely vegetated areas (10%) in the highlands; lakes (1%), wetlands (2%), grasslands (50%) and agricultural (12%) areas in the mid-high elevations (2200–5400 m a.s.l.); shrublands (13%) and various forest subcategories (7%) primarily concentrated in the lower northwest areas near the Amazon basin. The VUB includes four of Peru's 20 glacier mountain ranges, or "Cordilleras", distributed between zone 1 (Cordilleras Urubamba and Vilcabamba) and zone 3 (Cordilleras Vilcanota and La Raya). Total annual precipitation from Weather Research and Forecasting (WRF) model simulations (Fyffe et al., 2021; Potter et al., 2023) extended for the period 2013–2022 (Fig. 1e) averages 1003 mm per year, with a dry season from April to September and a wet season from October to March. Daily maximum temperatures remain relatively constant throughout the year (averaging 13–14.6°C across the entire catchment range), while mean daily minimum temperatures show stronger seasonality (−1.3°C in the dry season to 3.9°C in the wet season).

3. Methodology

3.1. Land cover classification

Landsat 7 and Landsat 8 Collection 2 Level−2 imagery from the U.S. Geological Survey were analysed from 2013 to 2022. This dataset provides atmospherically corrected surface reflectance products at 30 m spatial resolution. We analysed and processed 764 images in the Google Earth Engine platform (Gorelick et al., 2017). Due to the lack of image availability per month, we subset our images into four seasons: January to March (JFM), April to June (AMJ), July to September (JAS), and October to December (OND). The dataset was spatially constrained to the VUB boundary, including a 2 km buffer. After applying a cloud mask (Foga et al., 2017), we calculated the median values of the bands across all images in a given season and year to provide a reference multidate mosaic image. An initial visual inspection of the mosaiced median values revealed differences in image quality and quantity, where cloud presence was temporally and spatially variable (Fig. S1). To ensure sufficient data, we manually determined cloud cover thresholds per season (8–100%) (Table S1) and excluded 7 of 40 seasons where cloud presence remained high despite the thresholds. Based on the National Ecosystem Map (MINAM, 2018), eight main land cover classes were pre-defined: snow/ice, water, wetlands, agriculture, pastures, barren, shrubland, and forest (Table S2). In this study, wetlands were treated as a single land cover class and were not separated into wetland types.

Land cover classification was performed using a Random Forest model, an effective method for large-scale land cover classification (Gislason et al., 2006; Vega Isuhuaylas et al., 2018). For each season, a separate Random Forest model was run using the same fixed training dataset and configured with 30 decision trees to balance classification performance and computational efficiency. In total, 29 predictor variables were considered for classification (Table S3), including spectral indices derived from the minimum, maximum and median values of the seasonal image collections to assist land cover classification (Lee et al., 2018; Tsai et al., 2018), Landsat bands and topographic indices (elevation, slope, and aspect) computed from the SRTM V3 DEM at 30 m spatial resolution (Farr et al., 2007). For training, we established 80 fixed points (10 per class) across time (Fig. S2b), selected from randomly sampled points within areas with valid information across all seasons. Ten points per class were chosen after comparing three training dataset sizes, as this configuration

Table 1
Area and elevation ranges of the VUB and its zones.

Zone	Area (km^2)	% of VUB	Elevation range (m a.s.l.)	Location
VUB	11,048	100	1160–6324	-
Zone 1	3757	34	1160–6234	Northwest
Zone 2	2286	21	2955–4968	Centre
Zone 3	5006	45	3273–6324	Southeast
Zone 4	133	1.2	4732–5761	Northwest of zone 3

provided a better initial representation of the different classes (Supplement Material, section A.3). Training points were assigned to major land cover classes using the National Ecosystem Map (MINAM, 2018) and their class consistency was visually compared against Landsat true-colour composites for every one of the 33 seasonal mosaics. A sensitivity analysis comparing different number of decision trees for the model confirmed that 30 trees provided an adequate balance between classification performance and computational

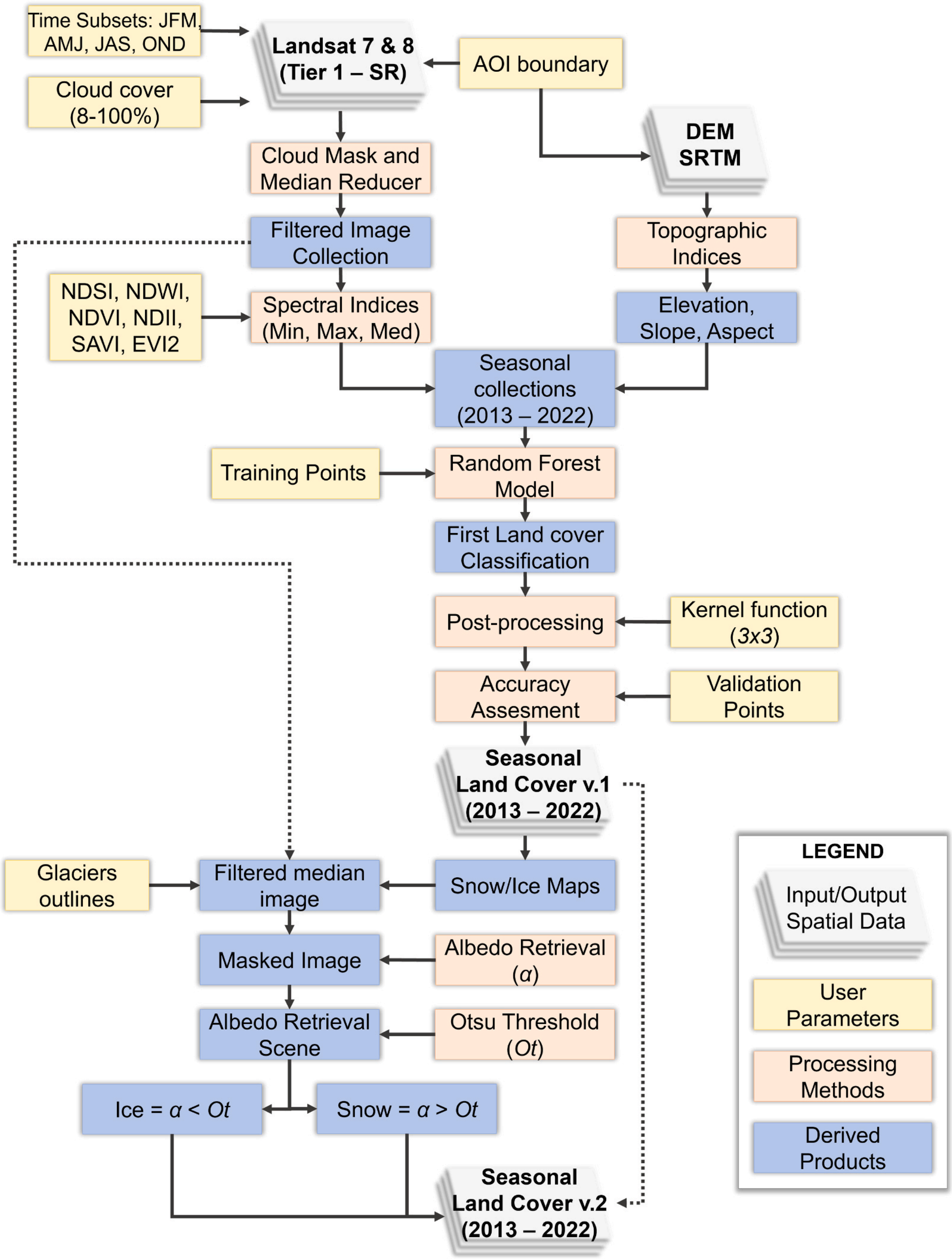

Fig. 2. Workflow for the land cover classification in VUB using Landsat 7 and 8 Tier 1 surface reflectance (SR). Seasons are three-month composites JFM (January-March), AMJ (April-June), JAS (July-September), and OND (October-December). AOI is the area of interest, including VUB extension and a 2 km buffer. Topographic indices include elevation, slope, and aspect computed from the SRTM V3 DEM. Spectral indices include NDSI (Normalised Difference Snow Index), NDWI (Normalised Difference Water Index), NDVI (Normalised Difference Vegetation Index), NDII (Normalised Difference Infrared Index), SAVI (Soil Adjusted Vegetation Index), and EVI2 (Enhanced Vegetation Index 2). Snow and ice are separated using albedo retrieval (α) and an Otsu threshold (Ot), where ice is classified as $\alpha < Ot$, and snow as $\alpha > Ot$.

efficiency (Table S4). Based on the first classification results, we merged agriculture and pasture into a single class due to similar spectral signature information (Fig. S3b and S4d-e). A majority filter using a weighted 3 × 3 Kernel function was then applied to reduce isolated pixels (Singh et al., 2022) caused by classification noise. In the absence of ground control points, we validated the classification results using an independent validation dataset generated by another operator from multiple true-colour satellite imagery (Landsat, Sentinel−2, and Google Earth, < 30 m spatial resolution) across seasons, with 2293 points in total (10 points per class and season). Land cover results were also compared with the areas from the national glacier (INAIGEM, 2018; 2023b) and wetland (INAIGEM 2023a) inventories. The classification achieved an overall accuracy of 0.74 and Kappa coefficient of 0.70, with improved performance during the dry season (mean overall accuracy = 0.76, Kappa coefficient = 0.71), and with lower performance in the wet seasons JFM and OND (mean overall accuracy = 0.72, Kappa coefficient = 0.67) (Fig. S6c) and in zones 1 and 2 where cloud presence was higher and image availability was lower, especially in zone 1 which had 223 images in the 33 seasons. The assessment of classification per land-cover class (Tables S6 and S7) showed that snow/ice and water had the highest performance, with F1-scores of 1.00 and 0.96, respectively. Wetlands showed high recall (0.92) and an F1-score of 0.79, while agriculture/pasture and shrub showed the lowest F1-scores (0.58 and 0.23, respectively. Further details on the validation are provided in the Supplementary Material section A.5.

After the first land cover classification, we further distinguished snow from ice applying the Albedo Retrieval approach (Liang, 2001; Naegeli et al., 2019) in combination with the Otsu method (Gaddam et al., 2022; Otsu, 1979), since snow and ice can have similar spectral response from Landsat bands. This method involves determining an optimal threshold within 0.25–0.55 based on the bimodal histogram of albedo pixel values derived from the seasonal median Landsat mosaics (see Supplementary Material section A.6). We derived the Snow Line Elevation (SLE) from the mapped snow by first calculating the area of snow-covered pixels and then determining the elevation at which the land area above can accommodate the snow-covered area, assuming that snow preferentially covers higher rather than lower elevations (Meier, 1975). Final land cover classification maps include the snow, ice, water, agriculture/pasture, wetland, barren, shrub and forest land cover classes for four three-month seasons (JFM, AMJ, JAS, OND) from 2013 to 2022. A summary of the full classification process is presented in Fig. 2, and further details on the methodology and classification model are provided in the Supplementary Materials section A.

3.2. Wetlands and land cover variability

The seasonal evolution of wetlands is related to that of all other land classes. We thus analyse both the temporal variability of all identified classes and their transitions into other classes to establish the overall picture of seasonal variability in land-surface change, against which to frame wetlands' temporal and spatial changes. We define inter-seasonal variability as the difference between a season's total area compared to the total area of the previous season. To identify land cover transitions across seasons, we quantified pixel transitions with Sankey diagrams estimated from a cross-tabulation matrix (Aldwaik and Pontius, 2012; Cuba, 2015; Li et al., 2020). First, we applied a confusion matrix to the land cover maps to estimate the pixels that *remained* in the same class or *transitioned* to another class in the following season. The pixel counts were converted into percentages and averaged per season and per zone. These transitions between classes were summarised using Sankey diagrams (Zhaoxu Liu, 2024).

To assess the link between snow and wetlands, we quantified their temporal frequency across VUB and its zones in the 33 seasons over the 2013–2022 period. Frequency was defined as the percentage of seasons during 2013–2022 in which a pixel was mapped as the same class. Frequency values were grouped into four categories using equal classification intervals to allow direct comparison between snow and wetland frequency classes: "rare" (3–9 seasons, 9–27% of the period), "occasional" (10–16, 30–48%), "frequent" (17–24, 52–73%), and "highly persistent" (25–33, 76–100%). Pixels present in two or fewer seasons were excluded. In addition, we quantified i) snow occurrence within and outside glacier outlines from the year 2020 (INAIGEM 2023b), ii) the overlap between snow and wetlands, and iii) the proximity of wetlands to glaciers. To further support the analysis of wetlands variability, statistical correlation analysis (Spearman's rank correlation coefficient) was applied between wetlands and i) climate data for air temperature and precipitation from gridded WRF data (Potter et al., 2023), spatially averaged over the VUB and the individual zones; and ii) other land cover classes, both at the inter-seasonal scale (26 values in 10 years). Further details on the climate data and correlations are provided in Supplementary Material sections B and F.

3.3. Wetland seasonal phases

We characterised four wetland seasonal phases based on the timing of drying and rewetting, calculated from the wetland areas in each season ($Wetland_{JFM}$, $Wetland_{AMJ}$, $Wetland_{JAS}$, $Wetland_{OND}$; km^2), with each value representing the median seasonal area from 2013 to 2022. These phases were established through initial assessments of wetland seasonality in small areas, alongside previous descriptions in the region (INAIGEM 2023a; Ross et al., 2023). We propose five parameters to characterise wetland seasonal phases based on their drying and recharge: overall dry-out (Do), beginning dry-out (Db), dry-out fraction (f), early recharge (Re), and total recharge (Rt).

$$Do = Wetland_{JAS} - Wetland_{JFM} \tag{1}$$

$$Db = Wetland_{AMJ} - Wetland_{JFM} \tag{2}$$

$$f = \frac{Db}{Do} \tag{3}$$

$$\mathrm{Re} = \frac{(Wetland_{OND} - Wetland_{JAS})}{|Do|} \tag{4}$$

$$Rt = \frac{(Wetland_{OND} - Wetland_{JFM})}{|Do|} \tag{5}$$

Here, *Do* (km^2) represents the total loss of wetland area through the end of the dry season, *Db* (km^2) captures the initial drying change of wetlands, and *f* represents the fraction of the initial dry-out (JFM-AMJ) relative to the total dry-out (JFM-JAS). The closer *f* is to 0, the slower the drying-out, while for delayed wetlands, $f < 0$. *Re* is the magnitude of the expected wetland recharge at the beginning of the wet season (OND-JAS) related to the total dry-out. *Rt* is the recharge of the wetland during OND compared to JFM, which filters inconsistent classifications due to lower JFM area values. The early wet season (OND) was considered to avoid classifying wetland phases with wrong signals due to low-quality or low-quantity information during the wet seasons.

Using these parameters, we grouped wetlands into four seasonal phase types (Fig. 3) per sub-basin in the VUB. Wetlands in the southern Peruvian Andes are expected to exhibit a drying phase, characterised by a reduction in saturated area from JFM to JAS, with $Do < 0$ and $Db \leq 0$. These were classified as "Seasonal dry-out" when $f \geq 0.30$ and as "Slow dry-out" when $0 \leq f < 0.30$, which corresponds to a slower change with AMJ area closer to JFM than JAS. Wetlands with $Do < 0$ and $Db > 0$ were labelled "Delayed dry-out", reflecting wetlands that remain saturated even after the end of the wet season (JFM). Phases with $Do \geq 0$ or with extreme rewetting ($Re < -0.10$ or $Rt > 3$) were grouped as "Inconsistent", since they are unlikely to represent a seasonal drying signal and may reflect mapping errors during wet seasons. These classifications were applied to the wetland seasonality of 615 sub-basins, delineated

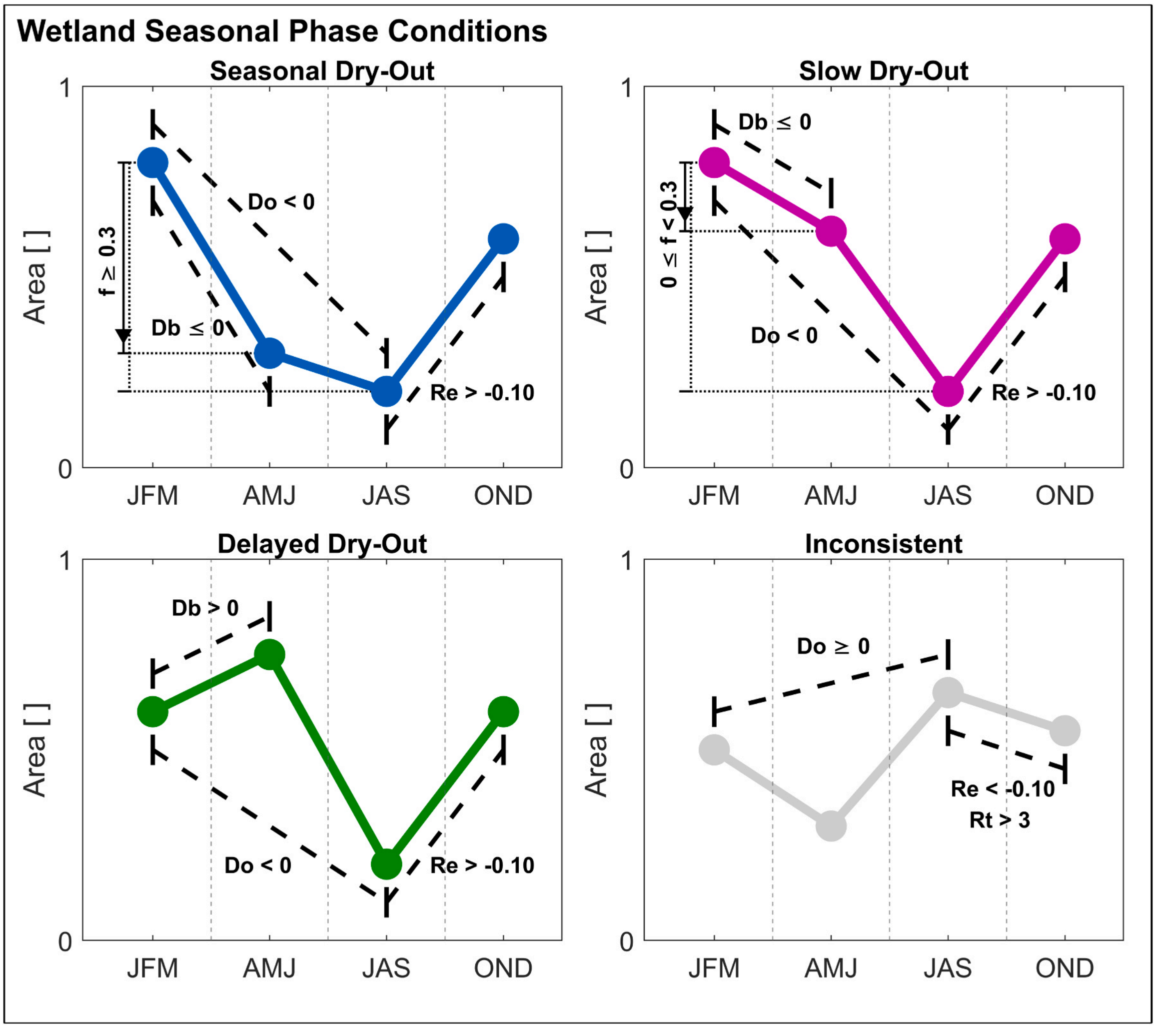

Fig. 3. Wetland classifications based on their seasonal area phase. We present four categories based on drying and rewetting conditions, following the timing of drying across four seasons (JFM, AMJ, JAS, OND). Parameters are: *Do*, overall dry-out; *Db*, beginning dry-out; *f*, dry-out fraction; *Re*, early recharge; and *Rt*, total recharge relative to JFM.

at Strahler 4 river order in the entire VUB using the SRTM V3 DEM. Only sub-basins with a complete wetland seasonality (i.e. with no gaps in any of the four median seasons) were assigned to one of the four wetland phase types; sub-basins containing wetlands with missing median data of one or more seasons were labelled as "Undefined".

4. Results

4.1. A new baseline of Andean land cover

Our mapping approach provides a new classification of land cover types and their seasonal and elevational variability in the VUB that performs well against validation data (Fig. S6) and improves the representation of glaciers and wetlands compared to the national inventories (INAIGEM, 2018; 2023a,) (see Supplementary Material section A.5). Between 2013 and 2022, the land cover of VUB was predominantly agriculture/pasture (52.5%), while wetlands (3.9%), snow (1.4%) and ice (0.4%) represented the smallest areas (Table 2). The land-cover elevation distribution is presented in Fig. 4. Snow, with its clear seasonality, spanned a broad elevation range from 3800 to 6300 m a.s.l., with a median elevation of 5037 m a.s.l. during AMJ, compared to 5400 m a.s.l. for ice. Compared to the other zones, the standard deviation of snow cover in zone 2 was higher, indicating greater temporal variability than in zones 1 and 3. Water bodies were present at higher elevations above 3500 m a.s.l., including lakes in proglacial valleys. Agriculture/pasture covered a wide elevation range across mid-to-low elevations (3500–4900 m a.s.l.). Wetlands were widely distributed up to 5400 m a.s.l. and were predominantly found in the higher areas of zone 3 and the mid-to-higher areas of zone 1. Shrubs and forests were less extensive and typically found together in elevations around 3150 m a.s.l. However, in zone 1, shrubs cover a larger area above 3600 m a.s.l. and forests are predominant below. Cloud cover and terrain shadows (4.1% of VUB) limited classification in some areas, resulting in unclassified or "NoData" areas near glaciers and steep terrain, largely in zone 1.

4.2. Inter-seasonal variability of Andean wetlands

Seasonal wetland patterns were consistent across VUB and its three zones (Fig. 5). Wetland extent in VUB decreased from 7.4% in JFM to 2.8% in JAS, followed by a slight rebound to 3.2% in OND (Fig. 5a), showing that the wetland saturated areas begin to reduce toward the end of the wet season (JFM), decreasing further through the dry months (AMJ, JAS). The sharpest reduction occurred in zones 2 and 3. An example of seasonal wetland maps is provided in Fig. S11. Wetlands and snow seasonal patterns were similar (Fig. 5b): snow area was highest at the end of the wet season (2.5% of VUB) and declined to 0.8% in AMJ, remaining near that level through the rest of the year, except in zone 3, where snow increased by 0.8% during JAS-OND. Precipitation, minimum temperature and average temperature (Fig. 5e, g, h) also exhibited seasonal patterns similar to those of wetlands. In contrast, the maximum temperature increased steadily from JFM to OND. Zone 3 had the greatest wetland extent and the coldest conditions, with slightly higher annual precipitation (1048 mm) than zones 1 (1035 mm) and 2 (835 mm). Only zone 3 registered average minimum temperatures below 0°C, occurring during the dry season. The inter-seasonal correlation analysis, presented in the Supplementary Material section F, further indicates that wetland variability covaries with precipitation, minimum and average temperatures across zones (Fig. S15).

Fig. 6 illustrates the seasonal transitions among major land cover classes in VUB. Agriculture/pasture showed the least change, with 73% of its pixels remaining the same on average from one season to the next, followed by barren soil at 60%. Snow cover is highly seasonal, and its seasonality shapes the changes into other classes: while snow pixels did not change much during the dry season (AMJ-JAS-OND), snow pixels transitioned to other classes mostly at the end of the wet season (JFM-AMJ), when 19% of the snow changed to agriculture/pasture and 23% to barren, with similar patterns across zones (Fig. 6). The seasonal transitions between snow and ice pixels were consistent between years. While 71% of ice pixels remained from AMJ to JAS, this dropped to 33% from JAS to OND when snow returned, and 40% of ice pixels transitioned into snow in VUB on average, with the highest rate observed in zone 3 (47%; Fig. S12d), as a result of snow accumulation over the glaciers. Most pixel-change patterns remained broadly consistent across zones.

Wetlands in VUB primarily transition to and from agriculture/pasture throughout the seasons. During the dry periods, 49% of the area remained as wetlands from AMJ to JAS, slightly increasing to 52% from JAS to OND, with zone 3 showing the highest values (59% and 69%, respectively; Fig. S12d). Large transitions from wetlands to agriculture/pasture occurred from AMJ to JAS (33%) and JAS to OND (24%). However, the highest transition of wetlands occurred at the beginning of the dry season (between JFM and AMJ), when over half (52%) of wetland area transitioned to agriculture/pasture, with similar values in zones 2 and 3 (54% and 55%, respectively; Fig. S12c-d). This change represents 416 km^2 of wetlands changing to agriculture/pasture between JFM and AMJ (~4% of the total area of the VUB), whereas during wet seasons (OND to JFM), ~420 km^2 of agriculture/pasture transitioned back into wetlands on

Table 2
Land cover area proportion per zone extension. Values represent the average area in percentage across all the seasons from 2013 to 2022.

Zone (km^2)	Snow (%)	Ice (%)	Water (%)	Wetland (%)	Agriculture/Pasture (%)	Barren (%)	Shrub (%)	Forest (%)	NoData (%)
VUB (11,048)	1.4	0.4	2.0	3.9	52.5	18.9	8.4	8.3	4.1
Zone 1 (3757)	2.2	0.4	1.6	3.6	36.7	14.9	11.8	19.6	9.2
Zone 2 (2286)	0.3	0.0	1.3	2.3	57.4	15.6	14.7	5.5	2.9
Zone 3 (5006)	1.4	0.7	2.6	5.0	62.0	23.4	3.1	1.0	0.9

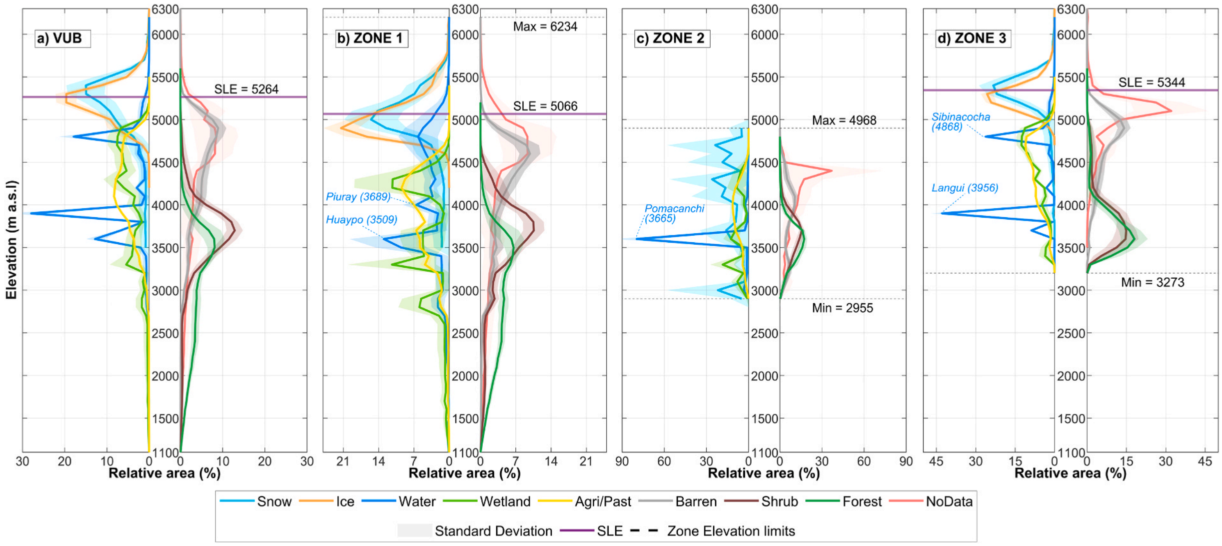

Fig. 4. Land cover distribution across 100 m elevation bands (m a.s.l.) for the entire VUB and its three zones. Relative area represents the proportion of the total area of each land cover class per elevation band. Solid colour lines represent the average relative area, and the shaded regions indicate their standard deviation over 10 years. Purple lines represent average Snow Line Elevation (SLE) derived from mapped snow using the Meier (1975) method. Dashed lines indicate the elevation limits of each zone; limits that coincide with the VUB boundary are not repeated (i.e. zone 1 minimum and zone 3 maximum elevations). Major lakes are annotated.

average (see Supplementary Material section D - Table S9). During the same periods, snow and barren areas had a much lower area exchange with wetlands (typically < 30 km^2 between seasons).

4.3. Andean wetlands dynamics and their links to the cryosphere

4.3.1. Wetland and snow temporal frequency

Fig. 7 shows the temporal frequency and spatial clustering of snow and wetlands across VUB and its three main zones and the smaller zone 4 sub-catchment. A summary of the snow and wetland presence per sub-region can be found in Supplementary Material section E (Table S10). In the VUB, 45% of the mapped snow between 2013 and 2022 was found over glaciers. Approximately 20% of total snow was "*highly persistent*" (present in more than three quarters of the seasonal Landsat mosaics), from which 96% was found over glaciers at elevations of ~5400 m a.s.l on average. At elevations < 4800 m a.s.l., snow was mostly of "*rare*" occurrence (present in 9–27% of scenes), suggesting uncommon or short-lived snowfall events in off-glacier areas that were captured at the time of the satellite overpass. This pattern is consistent within the higher elevation zone 3, with 63% of the total snow found on the glacier surface, with 31% of this "*highly persistent*" at high elevations (~5400 m a.s.l. on average). 45% of the total snow was "*rare*" in zone 3, often found along glacier edges, with only about one-third of those "*rare*" pixels occurring on-glacier. In the smaller zone 4, snow persistence was even higher, with more "*highly persistent*" (45%) and less "*rare*" (33%) snow.

"*Highly persistent*" wetlands were consistently found at the highest elevations (above 4600 m a.s.l., Table S10) and closer to glaciers than less persistent wetlands. "*Highly persistent*" wetlands (those present in more than three quarters of the seasonal Landsat mosaics) were more commonly found downstream of glacierised and snow-covered areas, occurring at an average distance of approximately 5.9 km from glaciers, compared to the "*frequent*" wetlands, which occurred on average 12.6 km from glaciers. In zone 3, 33% of wetlands were classified as "*frequent*" or "*highly persistent*", and therefore found in more than half of the scenes above 4500 m a.s.l. This pattern was more pronounced in zone 4, where 48% of wetlands were "*highly persistent*" and only 28% were "*rare*" (Fig. 7d). Importantly, a large proportion of wetland areas for the entire VUB (91%) were not "*highly persistent*". Across the VUB, 68% of the classified wetlands occurred in fewer than 30% of scenes, with a median elevation of ~3500 m a.s.l.

Although snow cover and wetlands rarely coincided spatially, their spatial proximity increased at higher elevations. As expected, snow consistently appeared in high-elevation areas, while wetlands concentrated more in mid-high-elevation valleys, separated by 500–800 m of elevation on average. Despite this proximity, snow presence over wetlands is scarce even above ~4500 m a.s.l., with only 0.5% of "*rare*" snow intersecting with "*highly persistent*" wetlands in less than 30% of seasons (Table S10).

4.3.2. The seasonal drying patterns of wetlands

Wetland seasonality was categorised based on the classification in Section 3.3 (Fig. 3), distinguishing four classes of wetlands (Fig. 8a). In the entire region, 366 (59.5%) of the 615 sub-basins were identified as including wetlands with a "seasonal dry-out" phase (Fig. 8b), where the reduction in the wetland saturated areas occurred after the end of the wet seasons (JFM) until JAS, with more of these wetlands found between zones 2 and 3, than in zone 1. Sixteen (2.6%) of the sub-basins were classified as "slow dry-out"

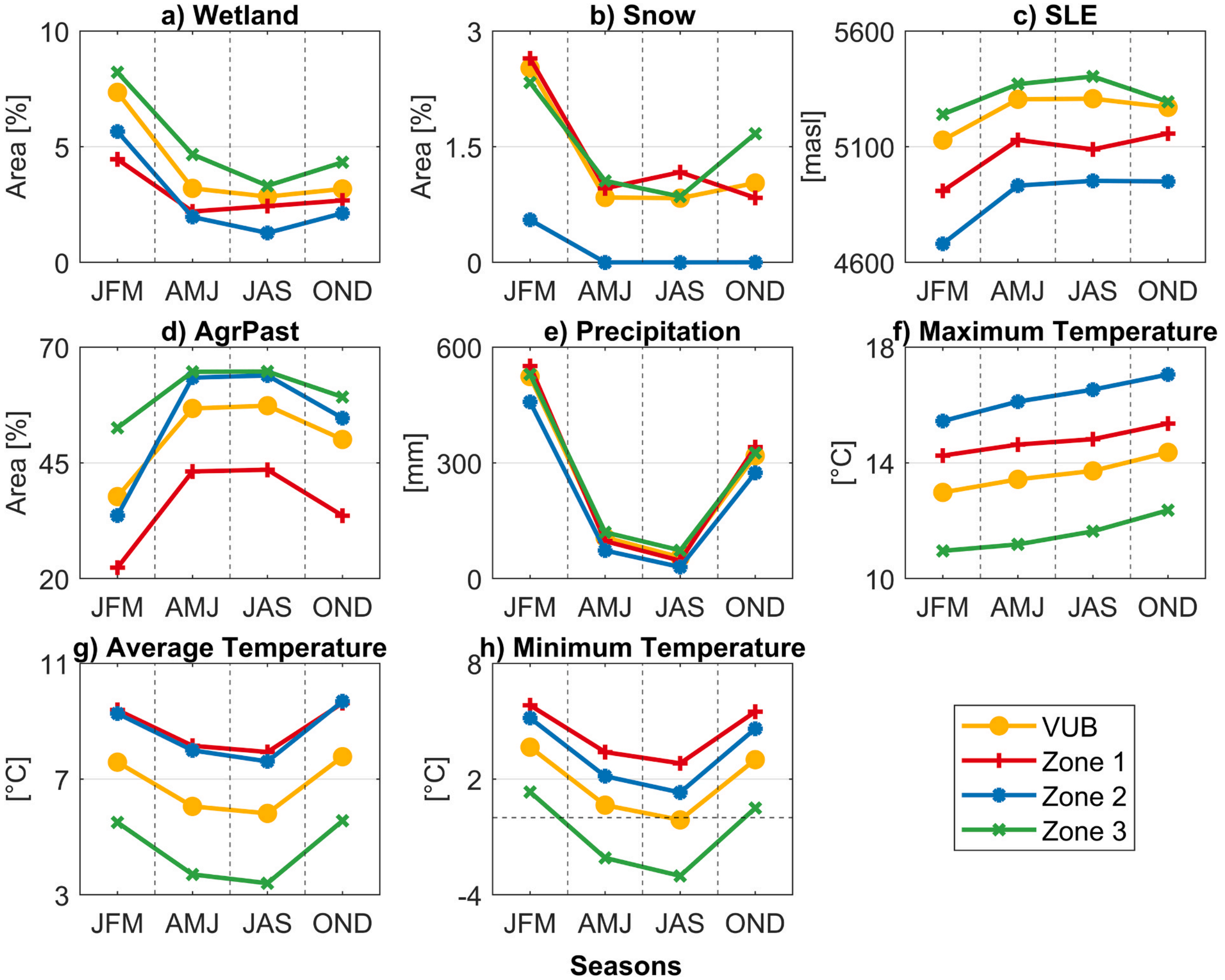

Fig. 5. Seasonal patterns of selected land cover, SLE and climate across VUB and its three zones from 2013 to 2022. Land cover median values are expressed as a percentage relative to the total area of each zone. SLE and climate variables represent the seasonal medians. Median values are calculated per season across all years.

wetlands, where the area declined in AMJ but reached its lowest area in JAS. "Delayed dry-out" wetlands, found in 13 (2.1%) of the 615 sub-basins, showed an increase in wetland area at the start of the drying season (AMJ), with prolonged saturated areas compared to previous months. Wetlands with an "inconsistent" seasonal phase comprised 183 (29.8%) of sub-basins. Finally, 37 (6%) sub-basins in the northeast VUB were defined as "Undefined", with mapped wetlands but without seasonality. Some of these last two cases could be due to errors in mapping wetlands during wet seasons (JFM and OND), when data availability is reduced.

Wetlands with a delayed or slow dry-out phase do not only exist in glacierised or snow-covered sub-basins, but they occur at significantly higher elevations (Fig. 8c; Table S12). Five of the 13 delayed dry-out wetlands (Table 3) occurred in sub-basins with glacier presence (10% cover of the sub-basin areas on average) and snow (18% cover of the sub-basin areas on average), and above 4200 m a.s.l. Six of 16 of the "slow dry-out" wetlands occurred in glacierised (11% cover on average) and snow-covered (15% cover on average) sub-basins above 4800 m a.s.l. Most of the "delayed dry-out" and "slow dry-out" wetlands were in zone 3, including three high-elevation cases in the smaller zone 4. Sub-basins with delayed dry-out wetlands also showed the highest occurrence of *highly persistent* wetlands (Fig. S13), which is logical since delayed dry-out wetlands have a larger proportion of wetland area that persists for most of the year.

5. Discussion

5.1. Spatio-Temporal Variability of Andean Wetlands

Here we present the first characterisation of the seasonal cycle of wetlands in the Andes. We show both a strong seasonality in wetland area, but also variability in the timing and magnitude of these seasonal patterns. Wetland seasonality in the Vilcanota-Urubamba Basin is characterised by a large area reduction during the dry season (Fig. 5), suggesting the drying-out of saturated

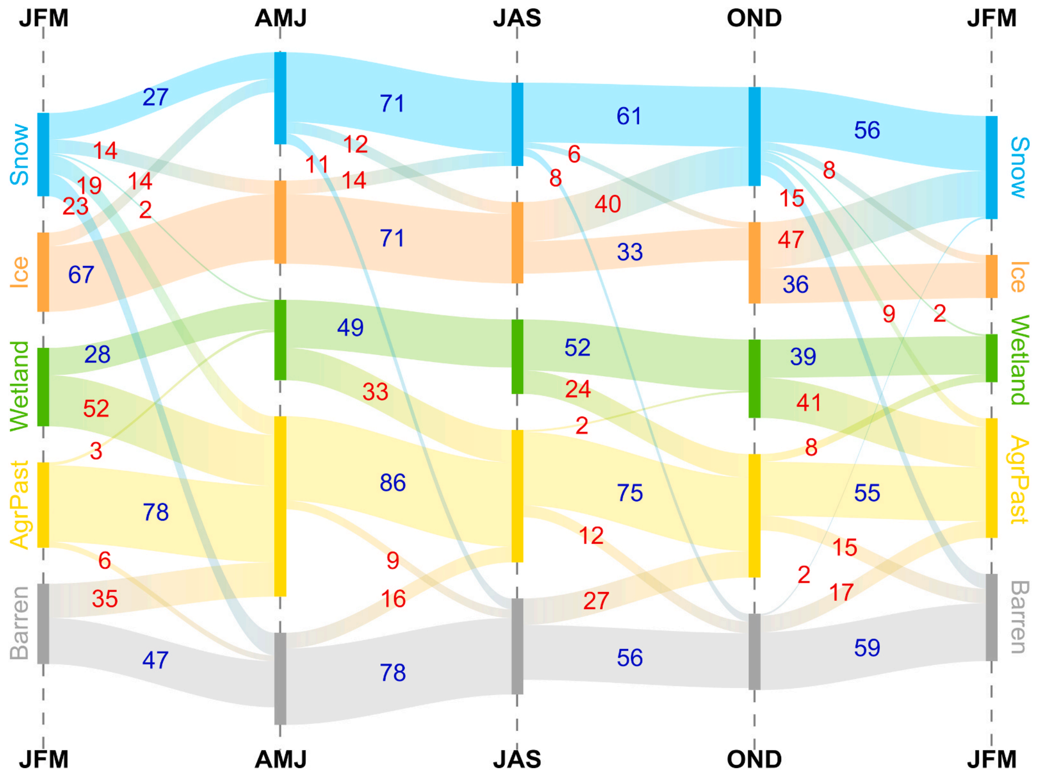

Fig. 6. Seasonal Sankey diagram of land cover pixel transitions in VUB. Labelled values represent the percentage of pixels of one class that remain the same (blue) or transition into another (red) between seasons, based on the pixel average over 2013–2022. Only dominant classes are shown; connectors below 2% and transitions to Water, Shrub, Forest and NoData classes were removed for clarity, so displayed values may not sum to 100%. The height of each bar is fixed and does not reflect the absolute area. Pixel transitions do not represent areas in absolute terms. For instance, a 52% transition of wetland pixels to agriculture/pasture (JFM to AMJ) corresponds to 417 km^2, whereas a 17% transition from agriculture/pasture to wetland (OND to JFM) corresponds to 429 km^2 (see Supplementary Material Section D). Transitions in VUB and its zones are provided in Fig. S12. Complete pixel transition matrices are provided in Data Availability.

surfaces. During the initial drying, large wetland areas shift into agriculture/pasture (∼400 km^2), eventually returning to wetlands during the wet seasons (Fig. 6). This transition into agriculture/pasture has never been shown before, and while providing a new picture of ecosystems' shift in the Andes, it also provides a novel baseline to investigate its causes. The wetland seasonal shift is relevant to livelihoods in the VUB headwaters, where livestock producers rely on wetlands and small ponds for water access and grazing (Muñoz et al., 2025). While it is consistent with localised observations of agriculture/pasture expansion during the dry seasons and drying out of wetlands surrounding pastures after the rainy season (Mazzarino, 2014), this is the first time that we show this process across three entire Cordilleras and quantify its extent.

Climate shapes wetland seasonal patterns through rain, evaporation, melt and vegetation processes (Saavedra et al., 2020; Barnett et al., 2005; Buytaert et al., 2011; Vuille et al., 2018). Despite this high-level understanding of broad controls, how those factors combine into shaping wetland dynamics and their mechanistic drivers remains unknown. Our correlation analysis (Fig. S15) found positive relationships between inter-seasonal wetland area changes and precipitation and average and minimum air temperatures at the scale of the VUB. This general pattern is found in zones 1 and 3, but with correlations changing sign in zone 2, where there are less precipitation, warmer conditions, and wetlands are less persistent compared to the other zones. This might suggest that wetland area expansion due to precipitation is a larger factor in wetland area change than drying due to evapotranspiration in warmer temperatures and presents a hypothesis that mechanistic modelling should prove or disprove. (Fig. S15). However, crucially, correlation analysis cannot disentangle processes and mechanistic drivers, and we caution against conclusive interpretations due to the limited temporal extent of our dataset.

Differences in the timing of wetland dry-out between sub-basins have allowed us to distinguish three main dry-out phases that might suggest distinct mechanisms of recharge and drying. Although "seasonal dry-out" phases were most common, "delayed dry-out" wetlands, with prolonged saturated areas and slower drying rates, were preferentially found at higher elevations, suggesting possible links to the cryosphere or high elevation processes. While the dry-out patterns of the "regular" wetlands (those we define as "seasonal dry-out") are consistent with wetlands in other Andean and lowland regions (de la Fuente et al., 2021; Zakharova et al., 2014), the slow and delayed dry-out have never been identified before.

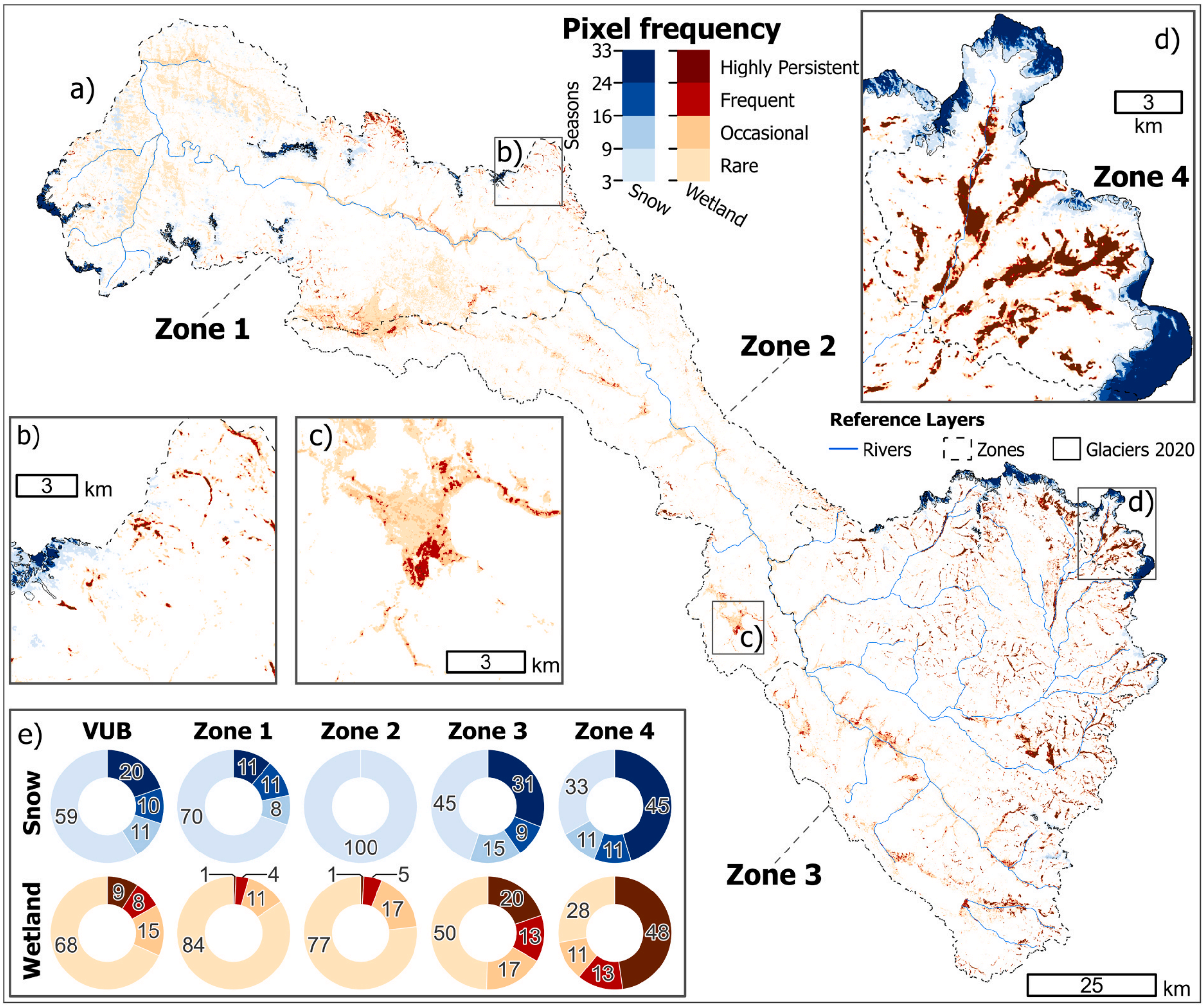

Fig. 7. Spatial frequency of snow and wetland presence across the VUB and its three zones and the smaller zone 4 sub-catchment. Snow (blue scale) and wetland (red scale) pixels are classified into frequency classes based on seasonal presence (33 seasons in total): Rare (3–9 seasons, or ~9–27% of the period), Occasional (10–16, or ~30–48%), Frequent (17–24, or ~52–73%), and Highly Persistent (25–33, or ~76–100%). Pixels with ≤ 2 seasons are excluded. Panel (a) shows results for the full VUB and zones, (b-d) illustrate examples across zones, (e) shows the percentages of the share of total persistent area (≥3 seasons) per frequency class and zones.

5.2. Wetland and cryosphere connectivity

More persistent wetlands are found predominantly at high elevations and concentrated down-valley from glacierised regions, near lakes and riparian systems, being located much closer to glaciers on average than less persistent wetlands (mean distance 5.5 km; Table S10). Despite this proximity, spatial overlap between mapped snow and wetlands remains minimal, with only 0.5% (Table S11) of snow covering wetland surfaces, even above 4500 m a.s.l. However, this low wetland-snow connectivity might be due to the temporal resolution of the satellite images that are unable to capture the occurrence of ephemeral snow, and therefore snowmelt contributions to wetlands may still occur at finer time scales than those obtainable through satellite-borne remote sensing from Landsat. Thin and ephemeral snowpacks of the Tropical Andes can accumulate and melt within hours to weeks, typically at elevations below 5000 m a.s.l. (Fyffe et al., 2021, 2025), and recent field observations have shown snow persisting over wetlands for short periods.

However, wetlands are likely to receive hydrological inputs from upstream snow and glacier melt, which alter their seasonal and annual water level fluctuations (Gribbin et al., 2024), as demonstrated for different climatic settings (Assini and Young, 2012; Carlson et al., 2020). To add complexity to this picture, although more common at higher elevations, delayed and slow dry-out wetlands are not exclusive to glacierised catchments (Fig. 8). Their occurrence in non-glacierised areas, such as zone 2, suggests that additional factors beyond a direct cryospheric influence might also affect the timing of wetland dry-out, such as the contribution from lateral slopes and groundwater inputs (Wunderlich et al., 2023).

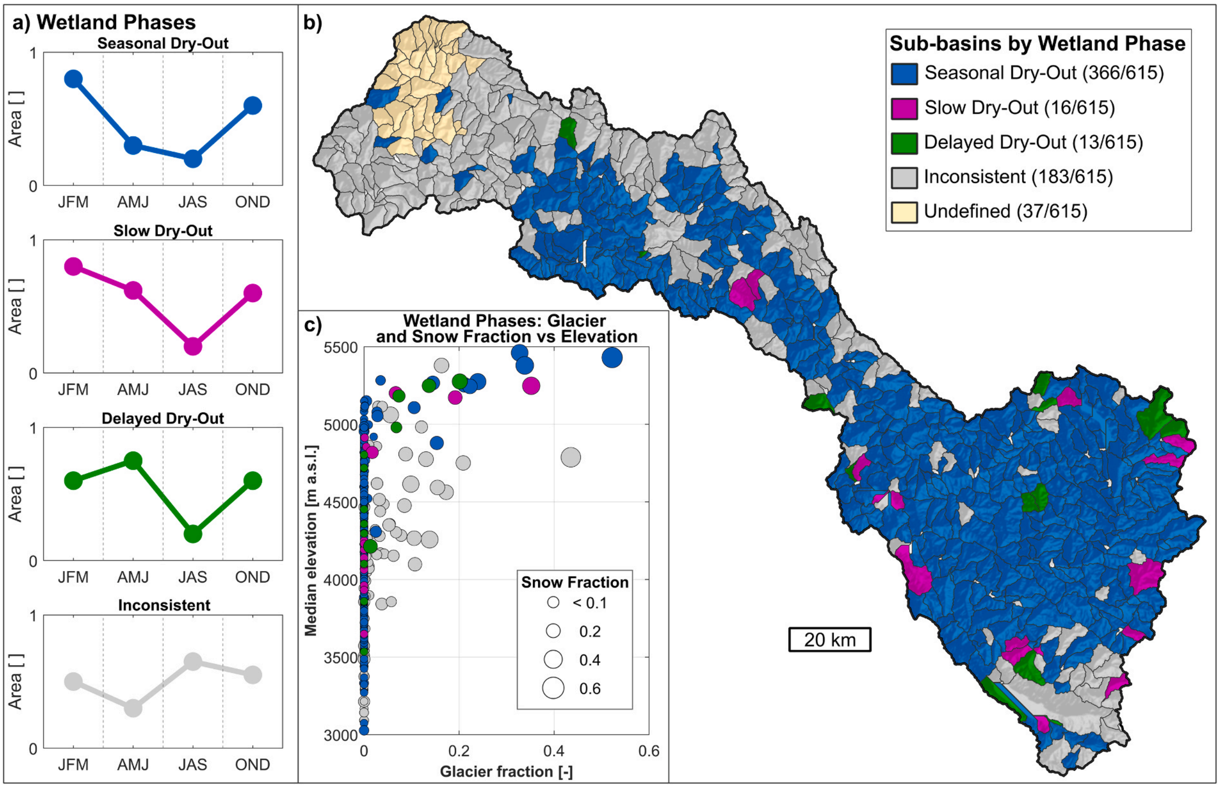

Fig. 8. Wetland seasonal phases across the VUB, 2013–2022. (a) shows the four wetland categories based on their seasonal phase, area and drying-out timing. (b) the categories applied to the 615 sub-basins in the VUB, including "Undefined" when mapped wetlands do not have a seasonality. (c) sub-basins classified by their wetland phase (colour), glacier fraction (x-axis) and snow fraction (marker sizes) distributed above 3000 m a.s.l. (Table S12). Glacier fraction was extracted from the 2020 glacier inventory (INAIGEM 2023b) and snow fraction was extracted from the snow frequency maps (Fig. 7). Wetlands fraction per sub-basin is presented in Fig. S14.

Table 3
Median elevation, glacier and snow fractions for delayed and slow dry-out wetlands. Only "delayed" and "slow dry-out" classes with glacier or snow fraction greater than zero are displayed to detail their cryospheric context.

Wetland Seasonal Phase	Basin-ID	Zone	Median Elevation (m a.s.l.)	Glacier (2020) fraction [-]	Snow (2013–2022) fraction [-]
Delayed dry-out	72	1	4214	0.0134	0.2082
	312	3	5276	0.2015	0.2672
	328	3	4980	0.0681	0.0930
	355	4	5183	0.0734	0.1466
	356	4	5249	0.1367	0.1983
Slow Dry-out	321	3	5201	0.0666	0.1739
	374	3	5248	0.3519	0.3737
	393	4	5173	0.1919	0.2022
	526	3	4856	0.0045	0.0001
	563	3	4914	0.0013	0.0045
	597	3	4819	0.0171	0.1448

To better understand the links between the cryosphere and wetlands at high elevations, we focus on the glacierised zone 4 sub-catchment in the Cordillera Vilcanota (Fig. 9), where high snow and wetlands persistence were identified. This catchment has a delayed dry-out wetland phase (Fig. 8), and this delay is consistent with local water table observations (Ross et al., 2023). We suggest that melt water contributes to the maintenance of the wetland areas in the early dry season (AMJ), since the slight increase in wetland area between JMF and AMJ corresponds with a decrease in snow-covered area (Fig. 9d), indicating that melt from snow and the newly exposed glacier ice is a likely contributor to inputs into the wetland system at this time of year. Evaporative fluxes might also play a role in controlling water fluxes from wetlands; for instance, evaporation-driven processes could affect groundwater (de la Fuente et al., 2021) and thus play a role in wetland recharge from lateral slope contributions (Cooper et al., 2019). This highlights the potential for more complex dynamics shaping wetlands than currently understood, especially at their transition zones with pastures (Fig. 9b).

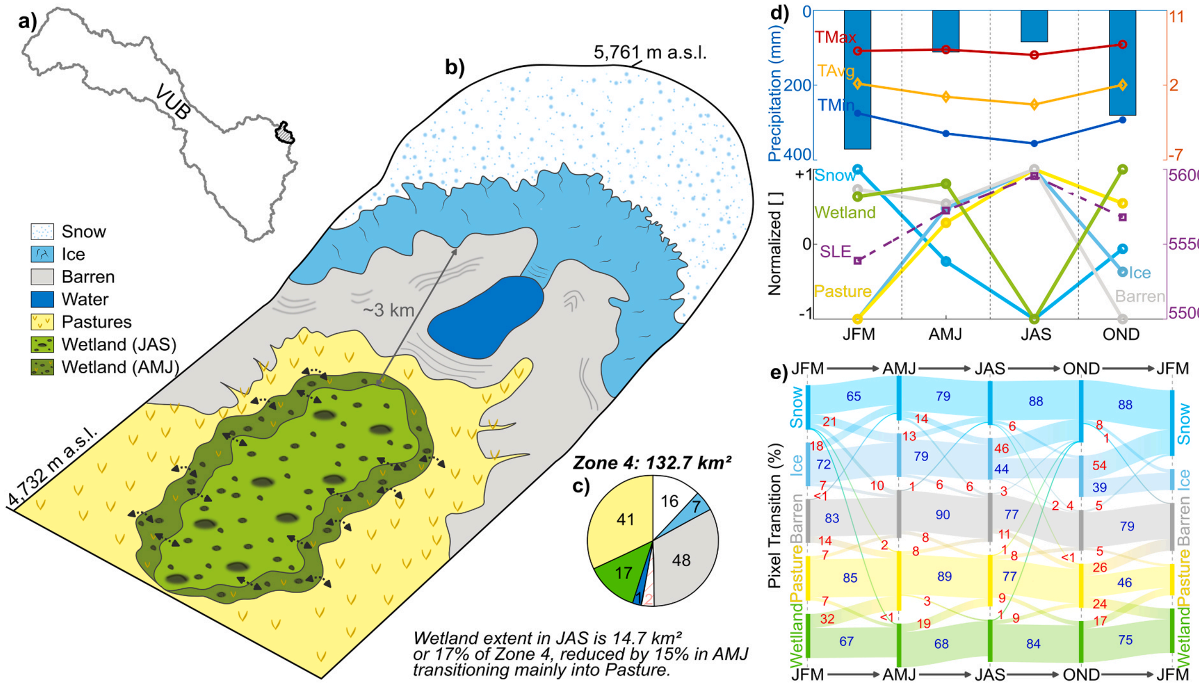

Fig. 9. Seasonal land cover dynamics in tropical high-mountain catchment. Case study in the Cordillera Vilcanota, (a) southeast VUB, including a (b) schematic land cover representation and (c) its composition as percentage of the total area. (d) Seasonal patterns of land cover (normalised anomalies scaled from −1 to 1 for comparison), climate, and snow line elevation. (e) Sankey diagram showing pixel transitions (%) between seasons.

5.3. Methodological Limitations

While our approach provides the first characterisation of wetland seasonality in the VUB, some methodological limitations must be considered. The land cover classification used Landsat imagery and cloud cover thresholds adjusted by season, which enabled consistent mapping during the wet and dry seasons. A first limitation is the similarity of spectral information among vegetated classes (Fig. S3 and S4), a common challenge in wetland mapping, as wetlands often exhibit similar spectral responses to surrounding land covers, reducing separability (Amani et al., 2018; Mahdavi et al., 2018). This limited separability is reflected in the low F1-scores for agriculture/pasture and shrub and in the lower precision of wetland classification (0.69), despite its high recall (0.92), indicating commission errors among vegetated classes. Although larger datasets generally improve classification accuracy (e.g. Ramezan et al., 2021), some classes can achieve high accuracy with smaller training samples (Phinzi et al., 2023). In this study, we prioritised balanced representation of land cover classes and the temporal distribution of the training dataset, accepting a reduced number of eligible points to ensure comparability across seasons. Additionally, although Otsu thresholding reduced the uncertainty of snow and ice pixels within the 0.25–0.55 albedo retrieval range, this separation could not be validated using our validation dataset (based on visual inspection) or field observation. Remaining errors in this range may affect the estimated snow and ice areas. The main limitation was the cloud presence during mapping the wet seasons. Retaining images with higher cloud cover preserved information but also increased residual cloud and terrain shadow effects, which can persist even after cloud masking (Lopes et al., 2020). These limitations were difficult to avoid given the basin's large spatial extent and high elevation range and contributed to classification errors and differences in accuracy assessment, particularly during the wet seasons (JFM and OND) and in zones 1 and 2 (Fig. S6).

Such mapping limitations can propagate into the analysis, by affecting the land cover area estimates, seasonal transitions and wetland phase classification, especially at the sub-basin scale. For instance, undetected clouds or residual shadows may introduce incorrect seasonal wetland areas and contribute to some "Inconsistent" phases, whereas high cloudiness and low image availability mainly generate data gaps, explaining the "Undefined" phases. To reduce the influence of these errors, wetland phases were defined from median seasonal areas from 2013 to 2022, representing typical seasonal phase rather than interannual variability. However, we need to accept slightly lower classification accuracy and more data gaps in order to map the seasonal fluctuations of wetlands in large basins. Applying the land cover classification approach over smaller areas and extended periods could reduce these limitations and enable assessment of interannual changes in wetland regimes at the sub-basin scale.

5.4. Building a way forward for mechanistic understanding of Andean wetland dynamics

In this study, we built a new baseline of wetland and landcover patterns in the VUB and explored their seasonal dynamics to reveal distinct dry-out timings of Andean wetlands and their transitions. Using three-month land cover maps from 2013 to 2022, we quantified Andean land cover seasonality, including wetlands seasonal phases across the VUB, with an overall accuracy of 0.74 against validation points independently collected from optical satellite imagery. This performance, in line with similar studies (Pizarro et al., 2022; Vega Isuhuaylas et al., 2018), demonstrates an improvement in wetland delineation relative to national inventories (see Supplementary Material section A.5). While we provide the first extensive quantification of wetland seasonality and seasonal shifts in the region by leveraging machine learning and high-resolution (30 m) satellite imagery, it is clear that the process-specific drivers and linkages that promote these patterns cannot be fully understood or resolved from seasonal remote sensing alone.

Different wetland seasonalities reflect coupled climatic and hydrological controls, adding complexity to the already under-researched understanding of how catchment processes (i.e. precipitation, snow, glacier melt, vegetation, and lateral slopes contribution) interact in high-Andean wetland systems (Polk et al., 2017; Ross et al., 2023), water storage and runoff (Drenkhan et al., 2023). Andean wetland persistence and seasonality can be broadly characterised from our approach, though cannot be fully understood at such coarse seasonal scales, as short events such as ephemeral snow can influence catchment hydrology (Fyffe et al., 2025) and wetlands. Addressing these uncertainties requires a combination of high-resolution remote sensing with ground-based monitoring and mechanistic modelling tools that operate at finer temporal resolutions (e.g. hourly or daily) to unravel the intricate interactions between the cryosphere, ecology, and hydrology in high-elevation catchments under ongoing climatic and cryospheric change. To date, despite local evidence and hypotheses of specific drivers and processes, no conclusive, deterministic investigation exists on the main causes of wetland existence and dry out at high elevations, nor on their links with snow and glaciers, calling for modelling investigations that can disentangle high elevation wetlands functioning.

Disentangling the hydrological dynamics of Andean wetlands and their drivers will aid our understanding of their response to future changes in climate and the cryosphere. Projected warming in the VUB is expected to result in warmer days and fewer frost days (Potter et al., 2023), with increased drought intensity and reduced snow precipitation. The latter, in particular, could significantly increase water stress during the dry months (Vuille et al., 2018; Poveda et al., 2020) and exacerbate the mass loss of the already small glaciers that can sustain high-mountain dry-season runoff (Fyffe et al., 2025). Our study has provided a novel, finely resolved baseline of wetlands and their changes that can now be used to build and validate numerical models of the Andean ecosystems, as well as test the hypotheses suggested by our study. The existence of slow and delayed dry-out wetlands calls for investigations on their drivers and differences to more traditional wetlands, and on their possible shifts to common wetlands and decline in persistence. Because these wetland phases are not restricted to glacierised catchments, their future sensitivity should be assessed not only in relation to glacier retreat, but also through potential shifts in precipitation, temperature and evapotranspiration. Our study paves the way for physically-based modelling studies to advance the understanding of Andean wetland functioning and the mechanisms that support their recharge, maintenance and dry out, and their future changes. This has implications for wetland ecosystem services because shifts in wetland dry-out timing can reduce the period when saturated areas remain available during the dry seasons, limiting their capacity for water regulation, grazing and agricultural activities, affecting livelihoods of highland communities, where adaptation strategies include land use management between pasture and high-Andean wetlands (Mazzarino, 2014; Postigo, 2014). Future work in the Tropical Andes should prioritise the improved quantification of the contribution from rain, snow, or glacier melt for wetland seasonality and the impact of higher temperatures on their variable dry-out phases.

6. Conclusions

In this study, we provide a novel baseline of seasonal maps of Andean land covers for the Vilcanota Urubamba Basin at a three-month scale from 2013 to 2022, and the first characterisation of wetlands extent and seasonality for the region. Wetlands occupy a small fraction of the total 11,000 km^2 basin, but span a large range of sub-regions and elevations, with the most persistent wetlands found at higher elevations and closer to glaciers. The seasonal dynamics of the wetlands are defined by the timing of their drying at the end of the wet season (March-April) and rewetting during the onset of the wet season later in the calendar year (October-December). As wetlands dry, almost half of them transform primarily into agricultural and pasture areas, eventually returning to wetlands during the wet season. Seasonal phases show that delayed and slow dry-out wetlands, which comprise only ~2% of the defined sub-catchments in the region, are not exclusive to glacierised catchments, but are predominantly found at higher elevations (> 4200 m a.s.l.) and close to glaciers and snow. At the three-month, seasonal scale, mapped snow and wetland areas show minimal spatial overlap, yet highly persistent wetlands (those occurring in > 76% of the available Landsat scenes) are common in catchments with greater snow and glacier presence, suggesting a direct link between wetlands and seasonal snow, which was not fully resolved in this study due to the frequency of satellite image acquisitions. Despite the limitations of optical satellite mapping in cloudy mountain regions and the need to use a small training dataset to allow consistency across seasons, our results provide the first quantification of seasonal wetland and land cover seasonalities at the scale of the entire Vilcanota-Urubamba and highlight the potential of complex dynamics driving wetland variability. This robust picture of seasonal wetland dynamics serves as a basis for future research on mountain wetlands, which should incorporate mechanistic modelling and catchment functioning, supported by higher-resolution remote sensing (sub-weekly) and new ground-based monitoring. This would allow building a full process understanding of wetland existence, persistence and changes, as well as the compounded drivers supporting their existence and dry-out, to establish their connectivity to the climate and cryosphere of the Tropical Andes, now and into the future with implications for wetland ecosystem services.

CRediT authorship contribution statement

Joshua Castro: Writing – original draft, Software, Methodology, Investigation, Formal analysis, Conceptualization. **Catriona L.**

Fyffe: Writing – review & editing, Supervision, Conceptualization. **Thomas E. Shaw:** Writing – review & editing, Supervision, Conceptualization. **Evan S. Miles:** Writing – review & editing, Supervision. **Emily Potter:** Writing – review & editing, Data curation. **Martin Hoelzle:** Writing – review & editing, Supervision. **Vinisha Varghese:** Writing – review & editing. **Francesca Pellicciotti:** Writing – review & editing, Supervision, Conceptualization.

Declaration of Competing Interest

The authors declare that they have no known competing financial interests or personal relationships that could have appeared to influence the work reported in this paper.

Acknowledgements

Joshua Castro acknowledges the support and funding of the Swiss Government Excellence Scholarships (ESKAS-Nr: 2022.0416) and the Doc. Mobility program by the University of Fribourg. Catriona Fyffe acknowledges support from the Marie Skłodowska-Curie Action project EPIC, which was funded by the European Union (grant number 101105480). Francesca Pellicciotti and Vinisha Varghese acknowledge support from the SNSF-funded PASTURE project, grant no. 202604. Emily Potter was jointly funded by a Leverhulme Trust ECR fellowship and NERC grant NE/X004031/1. We thank Miguel Vargas from the Universidad Nacional San Antonio Abad del Cusco for providing the validation points dataset used in this work.

Appendix A. Supporting information

Supplementary data associated with this article can be found in the online version at doi:10.1016/j.ejrh.2026.103808.

Data availability

Research Data and script is available in https://doi.org/10.5281/zenodo.18508189.

References

Aldwaik, S.Z., Pontius, R.G., 2012. Intensity analysis to unify measurements of size and stationarity of land changes by interval, category, and transition. Landsc. Urban. Plan. 106 (1), 103–114. https://doi.org/10.1016/j.landurbplan.2012.02.010.

Amani, M., Salehi, B., Mahdavi, S., Brisco, B., 2018. Spectral analysis of wetlands using multi-source optical satellite imagery. ISPRS J. Photogramm. Remote. Sens. 144, 119–136. https://doi.org/10.1016/j.isprsjprs.2018.07.005.

Assini, J., Young, K.L., 2012. Snow cover and snowmelt of an extensive high arctic wetland: spatial and temporal seasonal patterns. Hydrol. Sci. J. 57 (4), 738–755. https://doi.org/10.1080/02626667.2012.666853.

Barnett, T.P., Adam, J.C., Lettenmaier, D.P., 2005. Potential impacts of a warming climate on water availability in snow-dominated regions. In: Nature, 438. Nature Publishing Group, pp. 303–309. https://doi.org/10.1038/nature04141.

Bonshoms, M., Álvarez-Garcia, F.J., Ubeda, J., Cabos, W., Quispe, K., Liguori, G., 2020. Dry season circulation-type classification applied to precipitation and temperature in the Peruvian Andes. Int. J. Climatol. 40 (15), 6473–6491. https://doi.org/10.1002/joc.6593.

Buytaert, W., Cuesta-Camacho, F., Tobón, C., 2011. Potential impacts of climate change on the environmental services of humid tropical alpine regions. Glob. Ecol. Biogeogr. 20 (Number 1), 19–33. https://doi.org/10.1111/j.1466-8238.2010.00585.x.

Carlson, B.Z., Hébert, M., Reeth, C.Van, Bison, M., Laigle, I., Delestrade, A., 2020. Monitoring the seasonal hydrology of alpine wetlands in response to snow cover dynamics and summer climate: A novel approach with Sentinel-2. Remote. Sens. 12 (12). https://doi.org/10.3390/rs12121959.

Cavieres, L.A., Llambí, L.D., Anthelme, F., Hofstede, R., Arroyo, M.T.K., 2026. High-Andean. Vegetation Environmental Change A Continental Synthesis. https://doi.org/10.1146/annurev-environ-111523.

Cooper, D.J., Sueltenfuss, J., Oyague, E., Yager, K., Slayback, D., Caballero, E.M.C., Argollo, J., Mark, B.G., 2019. Drivers of peatland water table dynamics in the central Andes, Bolivia and Peru. Hydrol. Process. 33 (13), 1913–1925. https://doi.org/10.1002/hyp.13446.

Cuba, Nicholas, 2015. Research note: Sankey diagrams for visualizing land cover dynamics. Landsc. Urban. Plan. 139, 163–167. https://doi.org/10.1016/j.landurbplan.2015.03.010.

Drenkhan, F., Buytaert, W., Mackay, J.D., Barrand, N.E., Hannah, D.M., Huggel, C., 2023. Looking beyond glaciers to understand mountain water security. Nat. Sustain. 6 (2), 130–138. https://doi.org/10.1038/s41893-022-00996-4.

Drenkhan, F., Carey, M., Huggel, C., Seidel, J., Oré, M.T., 2015. The changing water cycle: climatic and socioeconomic drivers of water-related changes in the Andes of Peru. Wiley Interdiscip. Rev. Water 2 (6), 715–733. https://doi.org/10.1002/WAT2.1105.

Farr, T.G., Rosen, P.A., Caro, E., Crippen, R., Duren, R., Hensley, S., Kobrick, M., Paller, M., Rodriguez, E., Roth, L., Seal, D., Shaffer, S., Shimada, J., Umland, J., Werner, M., Oskin, M., Burbank, D., Alsdorf, D.E., 2007. The shuttle radar topography mission. Rev. Geophys. 45 (2). https://doi.org/10.1029/2005RG000183.

Fischer, M., Huss, M., Hoelzle, M., 2015. Surface elevation and mass changes of all Swiss glaciers 1980-2010. Cryosphere 9 (2), 525–540. https://doi.org/10.5194/tc-9-525-2015.

Foga, S., Scaramuzza, P.L., Guo, S., Zhu, Z., Dilley, R.D., Beckmann, T., Schmidt, G.L., Dwyer, J.L., Joseph Hughes, M., Laue, B., 2017. Cloud detection algorithm comparison and validation for operational Landsat data products. Remote. Sens. Environ. 194, 379–390. https://doi.org/10.1016/j.rse.2017.03.026.

de la Fuente, A., Meruane, C., Suárez, F., 2021. Long-term spatiotemporal variability in high Andean wetlands in northern Chile. Sci. Total. Environ. 756. https://doi.org/10.1016/j.scitotenv.2020.143830.

Fyffe, C.L., Potter, E., Fugger, S., Orr, A., Fatichi, S., Loarte, E., Medina, K., Hellström, R., Bernat, M., Aubry-Wake, C., Gurgiser, W., Perry, L.B., Suarez, W., Quincey, D.J., Pellicciotti, F., 2021. The Energy and Mass Balance of Peruvian Glaciers. J. Geophys. Res. Atmospheres 126 (23). https://doi.org/10.1029/2021JD034911.

Fyffe, C.L., Potter, E., Miles, E., Shaw, T.E., McCarthy, M., Orr, A., Loarte, E., Medina, K., Fatichi, S., Hellström, R., Baraer, M., Mateo, E., Cochachin, A., Westoby, M., Pellicciotti, F., 2025. Thin and ephemeral snow shapes melt and runoff dynamics in the Peruvian Andes. Commun. Earth Environ. 6 (1). https://doi.org/10.1038/s43247-025-02379-x.

Gaddam, V.K., Boddapati, R., Kumar, T., Kulkarni, A.V., Bjornsson, H., 2022. Application of "OTSU"—an image segmentation method for differentiation of snow and ice regions of glaciers and assessment of mass budget in Chandra basin, Western Himalaya using Remote Sensing and GIS techniques. Environ. Monit. Assess. 194 (5). https://doi.org/10.1007/s10661-022-09945-2.

Gislason, P.O., Benediktsson, J.A., Sveinsson, J.R., 2006. Random forests for land cover classification. Pattern Recognit. Lett. 27 (4), 294–300. https://doi.org/10.1016/j.patrec.2005.08.011.

Gorelick, N., Hancher, M., Dixon, M., Ilyushchenko, S., Thau, D., Moore, R., 2017. Google Earth Engine: Planetary-scale geospatial analysis for everyone. Remote. Sens. Environ. 202, 18–27. https://doi.org/10.1016/j.rse.2017.06.031.

Gribbin, T., Mackay, J.D., MacDonald, A., Hannah, D.M., Buytaert, W., Baiker, J.R., Montoya, N., Perry, L.B., Seimon, A., Rado, M., Arias, S., Vargas, M., 2024. Bofedal wetland and glacial melt contributions to dry season streamflow in a high-Andean headwater watershed. Hydrol. Process. 38 (8). https://doi.org/10.1002/hyp.15237.

IGN. (n.d.). *Carta Nacional del Perú 1:100,000 - Hidrografía*. Instituto Geográfico Nacional Del Perú (IGN) - Geoportal. Retrieved August 1, 2025, from https://www.idep.gob.pe/.

INAIGEM. (2018). *Inventario Nacional de Glaciares Las Cordilleras Glaciares del Perú 2018* (Instituto Nacional de Investigación en Glaciares y Ecosistemas de Montaña Biblioteca y Publicaciones, Ed.; Primera edición). https://hdl.handle.net/20.500.12748/57.

INAIGEM. (2023a). *Inventario Nacional de Bofedales del Perú 2023*. https://repositorio.inaigem.gob.pe/handle/16072021/466.

INAIGEM. (2023b). *Inventario Nacional de Glaciares y Lagunas de Origen Glaciar 2023*. https://repositorio.inaigem.gob.pe/items/7029db53-5118-4e93-8b2a-71e6e26db5f6.

Lee, J.K., Acharya, T.D., Lee, D.H., 2018. Exploring land cover classification accuracy of Landsat 8 image using spectral index layer stacking in hilly region of South Korea. Sens. Mater. 30 (12), 2927–2941. https://doi.org/10.18494/SAM.2018.1934.

Li, Z., Huang, S., Liu, D., Leng, G., Zhou, S., Huang, Q., 2020. Assessing the effects of climate change and human activities on runoff variations from a seasonal perspective. Stoch. Environ. Res. Risk Assess. 34 (3–4), 575–592. https://doi.org/10.1007/s00477-020-01785-1.

Liang, S., 2001. Narrowband to broadband conversions of land surface albedo I: Algorithms. Remote. Sens. Environ. 76 (2), 213–238. https://doi.org/10.1016/S0034-4257(00)00205-4.

Lopes, M., Frison, P.L., Crowson, M., Warren-Thomas, E., Hariyadi, B., Kartika, W.D., Agus, F., Hamer, K.C., Stringer, L., Hill, J.K., Pettorelli, N., 2020. Improving the accuracy of land cover classification in cloud persistent areas using optical and radar satellite image time series. In: Methods in Ecology and Evolution, 11. British Ecological Society, pp. 532–541. https://doi.org/10.1111/2041-210X.13359.

Mahdavi, S., Salehi, B., Granger, J., Amani, M., Brisco, B., Huang, W., 2018. Remote sensing for wetland classification: a comprehensive review. In: GIScience and Remote Sensing, 55. Taylor and Francis Inc, pp. 623–658. https://doi.org/10.1080/15481603.2017.1419602.

Maldonado Fonkén, M.S., 2014. Introd. bofedales Peruv. High. Andes 15 (Number 15). http://www.mires-and-peat.net/,ISSN1819-754X.

Mazzarino, M.M., 2014. Environ. Change agro-Pastor. livelihood Andes Peru.

Meier, M.F., 1975. Application of remote-sensing techniques to the study of seasonal snow cover. J. Glaciol. 15 (73), 251–265. https://doi.org/10.3189/S0022143000034419.

MINAM. (2018). *Mapa Nacional de Ecosistemas del Perú*. https://sinia.minam.gob.pe/mapas/mapa-nacional-ecosistemas-peru.

Muñoz, R., Santos, M.J., Castro-Álvarez, M.A., Mamani-Tapia, M.W., Miranda-Manrique, V., Huggel, C., 2025. The role of livelihood assets in shaping water security in mountain regions. Environ. Res. Lett. 20 (5). https://doi.org/10.1088/1748-9326/adc750.

Naegeli, K., Huss, M., Hoelzle, M., 2019. Change detection of bare-ice albedo in the Swiss Alps. Cryosphere 13 (1), 397–412. https://doi.org/10.5194/tc-13-397-2019.

Otsu, N., 1979. A Threshold Selection Method from Gray-Level Histograms. IEEE Trans. Syst. Man. Cybern. SMC-9 (1), 62–66. https://doi.org/10.1109/TSMC.1979.4310076.

Phinzi, K., Ngetar, N.S., Pham, Q.B., Chakilu, G.G., Szabó, S., 2023. Understanding the role of training sample size in the uncertainty of high-resolution LULC mapping using random forest. Earth Sci. Inform. 16 (4), 3667–3677. https://doi.org/10.1007/s12145-023-01117-1.

Pizarro, S.E., Pricope, N.G., Vargas-Machuca, D., Huanca, O., Ñaupari, J., 2022. Mapping Land Cover Types for Highland Andean Ecosystems in Peru Using Google Earth Engine. Remote. Sens. 14 (7). https://doi.org/10.3390/rs14071562.

Polk, M.H., Young, K.R., Baraer, M., Mark, B.G., McKenzie, J.M., Bury, J., Carey, M., 2017. Exploring hydrologic connections between tropical mountain wetlands and glacier recession in Peru's Cordillera Blanca. Appl. Geogr. 78, 94–103. https://doi.org/10.1016/j.apgeog.2016.11.004.

Postigo, J.C., 2014. Perception and Resilience of Andean Populations Facing Climate Change. J. Ethnobiol. 34 (3), 383–400. https://doi.org/10.2993/0278-0771-34.3.383.

Potter, E.R., Fyffe, C.L., Orr, A., Quincey, D.J., Ross, A.N., Rangecroft, S., Medina, K., Burns, H., Llacza, A., Jacome, G., Hellström, R., Castro, J., Cochachin, A., Montoya, N., Loarte, E., Pellicciotti, F., 2023. A future of extreme precipitation and droughts in the Peruvian Andes. Npj Clim. Atmos. Sci. 6 (1). https://doi.org/10.1038/s41612-023-00409-z.

Poveda, G., Espinoza, J.C., Zuluaga, M.D., Solman, S.A., Garreaud, R., van Oevelen, P.J., 2020. High Impact Weather Events in the Andes. In: Frontiers in Earth Science, 8. Frontiers Media S.A. https://doi.org/10.3389/feart.2020.00162.

Ramezan, C.A., Warner, T.A., Maxwell, A.E., Price, B.S., 2021. Effects of Training Set Size on Supervised Machine-Learning Land-Cover Classification of Large-Area High-Resolution Remotely Sensed Data. Remote. Sens. 13 (3), 368. https://doi.org/10.3390/rs13030368.

Ross, A.C., Mendoza, M.M., Drenkhan, F., Montoya, N., Baiker, J.R., Mackay, J.D., Hannah, D.M., Buytaert, W., 2023. Seasonal water storage and release dynamics of bofedal wetlands in the Central Andes. Hydrol. Process. 37 (8). https://doi.org/10.1002/hyp.14940.

Saavedra, M., Junquas, C., Espinoza, J.C., Silva, Y., 2020. Impacts of topography and land use changes on the air surface temperature and precipitation over the central Peruvian Andes. Atmos. Res. 234. https://doi.org/10.1016/j.atmosres.2019.104711.

Seehaus, T., Malz, P., Sommer, C., Lippl, S., Cochachin, A., Braun, M., 2019. Changes of the tropical glaciers throughout Peru between 2000 and 2016 - Mass balance and area fluctuations. Cryosphere 13 (10), 2537–2556. https://doi.org/10.5194/tc-13-2537-2019.

Singh, M.P., Gayathri, V., Chaudhuri, D., 2022. A Simple Data Preprocessing and Postprocessing Techniques for SVM Classifier of Remote Sensing Multispectral Image Classification. IEEE J. Sel. Top. Appl. Earth Obs. Remote. Sens. 15, 7248–7262. https://doi.org/10.1109/JSTARS.2022.3201273.

Taylor, L.S., Quincey, D.J., Smith, M.W., Potter, E.R., Castro, J., Fyffe, C.L., 2022. Multi-Decadal Glacier Area and Mass Balance Change in the Southern Peruvian Andes. Front. Earth Sci. 10. https://doi.org/10.3389/feart.2022.863933.

Tsai, Y.H., Stow, D., Chen, H.L., Lewison, R., An, L., Shi, L., 2018. Mapping Vegetation and Land Use Types in Fanjingshan National Nature Reserve Using Google Earth Engine. Remote. Sens. 10 (6). https://doi.org/10.3390/rs10060927.

Turpo Cayo, E.Y., Borja, M.O., Espinoza-Villar, R., Moreno, N., Camargo, R., Almeida, C., Hopfgartner, K., Yarleque, C., Souza, C.M., 2022. Mapping Three Decades of Changes in the Tropical Andean Glaciers Using Landsat Data Processed in the Earth Engine. Remote. Sens. 14 (9). https://doi.org/10.3390/rs14091974.

Vega Isuhuaylas, L.A., Hirata, Y., Santos, L.C.V., Torobeo, N.S., 2018. Natural forest mapping in the Andes (Peru): A comparison of the performance of machine-learning algorithms. Remote. Sens. 10 (5). https://doi.org/10.3390/rs10050782.

Vuille, M., Carey, M., Huggel, C., Buytaert, W., Rabatel, A., Jacobsen, D., Soruco, A., Villacis, M., Yarleque, C., Elison Timm, O., Condom, T., Salzmann, N., Sicart, J.E., 2018. Rapid decline of snow and ice in the tropical Andes – Impacts, uncertainties and challenges ahead. In. In: Earth-Science Reviews, 176. Elsevier B.V, pp. 195–213. https://doi.org/10.1016/j.earscirev.2017.09.019.

Wunderlich, W., Lang, M., Keating, K., Perez, W.B., Oshun, J., 2023. The role of peat-forming bofedales in sustaining baseflow in the humid puna. J. Hydrol. Reg. Stud. 47. https://doi.org/10.1016/j.ejrh.2023.101394.

Zakharova, E.A., Kouraev, A.V., Rémy, F., Zemtsov, V.A., Kirpotin, S.N., 2014. Seasonal variability of the Western Siberia wetlands from satellite radar altimetry. J. Hydrol. 512, 366–378. https://doi.org/10.1016/j.jhydrol.2014.03.002.

Zhaoxu Liu. (2024). sankey plot. In https://www.mathworks.com/matlabcentral/fileexchange/128679-sankey-plot. MATLAB Central File Exchange.